

Cluster model calculations with non-local screening channels of metallic and insulating VO₂

R.J.O. Mossaneck and M. Abbate*

*Departamento de Física, Universidade Federal do Paraná,
Caixa Postal 19091, 81531-990 Curitiba PR, Brazil*

We studied the changes in the electronic structure of VO₂ across the metal-insulator transition. The main technique was cluster model calculations with non-local screening channels. The calculation included a screening from a coherent state at the Fermi level in the metallic phase, and a screening from a Hubbard charge fluctuation within the V-V dimer in the insulating phase. The calculation results are compared to previous photoemission and X-ray absorption spectra. The coherent feature at the Fermi level in the metallic phase is due to the coherent screening. But the Hubbard screened state in the insulating phase appears at higher energies opening the band gap. The changes in the electronic structure of VO₂ are thus related to the non-local screening channels.

PACS: 79.60.Bm; 78.70.Dm; 71.30.+h

Keywords: VO₂, electronic structure, metal-insulator transition, cluster model, band structure, photoemission, X-ray absorption, non-local screening, V-V dimmers

I. Introduction

Vanadium dioxide undergoes a first order metal-insulator transition [MIT] at about 340 K [1,2]. Above the transition temperature, VO₂ is a paramagnetic metal with a tetragonal symmetry. Below the critical temperature, it becomes a diamagnetic semiconductor with a monoclinic symmetry. The low temperature phase is characterized by the formation of distinct V-V dimmers along the crystal c-axis. The electronic structure of VO₂ was first described in terms of molecular orbital theory [3]. This description was based on a single V⁴⁺ ion surrounded by an edge sharing O²⁻ octahedra. The crystal field splits the V 3d levels into three low energy t_{2g} levels and two high energy e_g levels. The lowest energy partially filled t_{2g} level, which connects the V-V dimmers, forms the so-called d_{||} band. The V-V dimerization splits the d_{||} band, forms a localized singlet, and opens a band gap [3].

VO₂ was studied using photoemission (PES) [4,5] and X-ray absorption (XAS) [6,7] spectroscopy. The electronic structure was studied using band structure [8-10] and cluster model [11,12] calculations. These early calculations were in qualitative agreement with the experimental results, and corroborated the main ideas of the molecular orbital model. But they failed to reproduce the value of the band gap, and the *coherent* and *incoherent* structures in the PES spectra [13]. A recent photoemission work [14], showed drastic changes in the coherent and incoherent structures across the MIT. In an effort to reproduce these features, many works were carried out using the GW [15] and DMFT [16,17] methods. These provided a better estimate of the band gap and reproduced the coherent and incoherent features. But they failed to explain key features in

the unoccupied electronic states mapped by X-ray absorption [18].

We studied here the changes in the electronic structure of VO₂ across the MIT using cluster model calculations. The present cluster model is similar to that used to study the electronic structure of Mn compounds [19,20]. Aside from the usual local ligand screening, we added a different non-local screening channel to each phase. In the metallic phase, we included a screening from a coherent state at the Fermi level [21,22]. We found that both coherent and incoherent structures present in the V 3d band are well screened states, while the poorly screened state appears at much higher energies. In the insulating phase, we added a Hubbard screening from the V neighbor in the V-V dimer [23,24]. As a result, the V 3d occupied band is now formed by one well screened state, while the other is pushed close to the poorly screened state. In addition, this model reproduces the splitting observed experimentally in the d_{||} unoccupied band. This shows that the changes in the electronic structure are related to the non-local screening channels.

II. Calculation details

A. Band structure

The band structure was calculated using the Full Potential Linear Muffin Tin Orbital method [25]. The exchange and correlation potential was calculated using the Vosko approximation. The metallic phase was calculated in the tetragonal structure (space group P4₂/mnm). The lattice parameters were $a = 4.530 \text{ \AA}$ and $c = 2.896 \text{ \AA}$ and the atomic positions were V = (0.000, 0.000, 0.000) and O = (0.305, 0.305, 0.000). The self-consistent potential and the density of states were calculated using 24 irreducible **k**-points. The insulating phase was calculated in the monoclinic structure (space

group P2₁/c). The lattice parameters were $a = 5.743 \text{ \AA}$, $b = 4.517 \text{ \AA}$, $c = 5.375 \text{ \AA}$ and $\beta = 121.56^\circ$. The atomic positions were $V = (0.233, 0.024, 0.021)$, $O1 = (-0.118, 0.288, 0.272)$ and $O2 = (0.399, 0.315, 0.293)$. The self-consistent potential and the density of states were calculated using 80 irreducible \mathbf{k} -points.

B. Cluster Model

The cluster model was solved using the standard configuration interaction method [26,27]. The cluster considered here consisted of a V^{4+} ion surrounded by a regular O^{2-} octahedra. The ground state was expanded in the $3d^1$, $3d^2\bar{L}$, $3d^3\bar{L}^2$, $3d^4\bar{L}^3$, $3d^5\bar{L}^4$ configurations, where \bar{L} denotes an O 2p hole [11,12]. The main parameters of the model were the charge-transfer energy Δ , the d-d Coulomb energy U , and the p-d transfer integral T_σ [26,27]. The multiplet splitting was given in terms of the crystal field splitting $10Dq$, the p-p transfer integral $pp\pi$ - $pp\sigma$, and the intra-atomic exchange J , as outlined in our early work on Mn compounds [19,20]. The addition (removal) state was obtained by adding (removing) an electron to the ground state. Finally, the spectral weight was calculated using the sudden approximation [19,20]. The main cluster model parameters were $\Delta = 2.0 \text{ eV}$, $U = 4.5 \text{ eV}$ and $T_\sigma = 3.2 \text{ eV}$. The multiplet splitting parameters were $J = 0.4 \text{ eV}$, $10Dq = 1.9 \text{ eV}$ and $pp\pi$ - $pp\sigma = 1.0 \text{ eV}$. These parameters give the best results and are also in agreement with previous cluster model works [11,12].

C. Coherent screening

The metallic phase calculation included a screening from a coherent state at the Fermi level. This non-local screening was recently proposed in a hard X-ray photoelectron study of V_2O_3 [21], following the original idea in an early study of core-level photoemission in Ni [22]. The charge fluctuations of this screening are represented schematically in the upper part of Fig. 1. The charge-transfer energy from the coherent state was Δ^* and the transfer integral was T^* [21,22]. The metallic ground state was thus expanded in the $3d^1$, $3d^2\bar{C}$, $3d^3\bar{L}$, $3d^3\bar{C}^2$, $3d^3\bar{C}\bar{L}$, $3d^3\bar{L}^2$, etc. configurations (where \bar{C} denotes a hole in the coherent band) [21]. The energy level diagram of the configurations of the metallic ground state is given in the lower part of Fig. 1 (the multiplet splitting was not included for simplicity). The charge-transfer energy from the coherent state in the metallic phase was set to $\Delta^* = 0.6 \text{ eV}$. The transfer integral involves V 3d-V 3d fluctuations at the Fermi level and was set to $T^* = 0.3 \text{ eV}$. These parameters are similar to those used to explain the core-level spectra of metallic V_2O_3 [21].

D. Hubbard screening

The insulating phase calculation included a Hubbard screening from the neighboring $d_{||}$ electron. This charge fluctuation within the V-V dimer is depicted schematically in the upper part of Fig. 2. The charge-transfer energy for this fluctuation becomes $U = 4.5 \text{ eV}$ and the corresponding transfer integral is T' [23,24]. The insulating ground state was then expanded in the $3d^1$, $3d^2\bar{D}$, $3d^2\bar{L}$, $3d^3\bar{D}\bar{L}$, $3d^3\bar{L}^2$, etc. configurations (where \bar{D} denotes a hole in the neighboring V site within the V-V dimer). The energy level diagram of the configurations in the insulating ground state is shown in the lower part of Fig. 2 (the multiplet splitting were not included for simplicity). The transfer integral involves V 3d-V 3d fluctuations within the V-V dimer and was set to $T' = 2.5 \text{ eV}$. The larger value of T' reflects the larger overlap between the $d_{||}$ states within the V-V dimer.

III. Results

Figure 3 shows the removal states of VO_2 decomposed in the main final state configurations. In the metallic phase, the coherent part, around -0.4 eV , is mostly formed by the $3d^1\bar{C}$ state, with 23 %, while the incoherent part, about -1.6 eV , is mainly formed by the $3d^1\bar{L}$ state, with 35 %. Both the coherent and incoherent parts correspond to the so called well screened states. The screening charge in the coherent part comes from a coherent state at the Fermi level, whereas the screening charge in the incoherent part comes from O 2p states in the ligand band. The so-called poorly screened state, around -7.1 eV , is mainly composed by the $3d^0$ state, with 30%. The well screened states $3d^1\bar{C}$ and $3d^1\bar{L}$ appear close to the Fermi level because both Δ and Δ^* are relatively small, while the poorly screened state $3d^0$ appears deeper in energy because of the relatively large value of U .

In the insulating phase, the so called lower Hubbard band around -0.9 eV is actually formed by the $3d^1\bar{L}$ state with 29 %. This corresponds to a well screened state with the screening charge coming from O 2p states in the ligand band. The other well screened state in this case, $3d^1\bar{D}$, appears away from the Fermi level, around -5.5 eV . The screening charge of this state comes from the adjacent $d_{||}$ electron within the V-V dimer. The charge fluctuation from the single V neighbor costs U and pushes the state towards higher energies. Finally, the poorly screened state, which appears about -6.8 eV , is mostly composed by the $3d^0$ state. This state appears at higher energies because of the relatively large value of U .

These results show that VO_2 is in a heavily mixed charge-transfer regime, which was to be expected because $\Delta < U$ and T is relatively large. The well screened $3d^1\bar{L}$ states appear close to the

Fermi level, around Δ , whereas the poorly screened $3d^0$ state appears at higher energy, about U . This interpretation is qualitatively supported by a valence band resonant photoemission [28]. The differences between the metallic and insulating phase are mostly due to changes in the non-local screening channels. In the metallic phase, the screening from coherent states $3d^1\bar{C}$ appears close to the Fermi level, because the charge fluctuation Δ^* costs relatively little energy. In the insulating case, the screening from the neighboring V site $3d^1\bar{D}$ appears at higher energy, because the charge fluctuation costs a relatively large U . Finally, the usual screening from O 2p states $3d^1\bar{L}$ form a spectator state in the metallic phase, and becomes the lowest energy removal state in the insulating phase.

Figure 4 compares the results from the band structure and the cluster model calculations. As expected, the total DOS in the metallic phase is continuous at the Fermi level. The DOS in this region are mainly formed by V 3d states, although there are also considerable O 2p states from the covalent mixing. The V 3d states are split by the crystal field generated by the oxygen octahedra. The structure from -0.5 to 2.0 eV is related to the V t_{2g} states while the structure from 2.5 to 5 eV corresponds to the V e_g states. The $d_{||}$ band, in this case, is mostly spread across the Fermi level from -0.5 to 1.0 eV. Finally, the charge fluctuations predicted by the band structure calculation are of the d-d type.

The cluster model calculation is a combination of the removal and addition states. The discrete transitions of the model were broadened by a Gaussian function. The removal state presents two structures at -0.4 and -1.6 eV, which correspond to the well screened $3d^1\bar{C}$ and $3d^1\bar{L}$ states, respectively. The poorly screened $3d^0$ transition, which corresponds to the lower Hubbard band, appears deeper in energy. The addition state consists of various structures corresponding to the different $3d^2$ final state configurations. The structures at 0.6 and 1.0 eV represent the addition of a majority and minority t_{2g} electron. The smaller peak, with a partial overlap at 1.0 eV, corresponds to the addition of a $d_{||}$ electron. Finally, the structures at 3.3 and 3.7 eV represent the addition of a majority and minority e_g electron. The charge fluctuations involve transitions from a coherent $3d^1\bar{C}$ state to a $3d^2$ state (the precise nature of the charge fluctuations is related to the orbital population in each phase [29]).

The total DOS in the insulating phase shows a semi-metallic character, with a pseudo-gap at the Fermi level. The absence of a true band gap is attributed to electron correlation effects beyond the LDA approach. The peak around -0.2 eV is related to the occupied part of the $d_{||}$ band, whereas the structure at 2.0 eV corresponds to the

unoccupied part of the $d_{||}$ band. It is worth noting that the covalent O 2p character mixed in the $d_{||}$ band is particularly small. The overall splitting of the $d_{||}$ band, which is mainly caused by the lattice distortion within LDA, is about 2.0 eV. There are only minor changes in the t_{2g} band, and the e_g band becomes slightly broader in this phase. The charge fluctuations across the Fermi level continue to be of the d-d type, as in the metallic phase.

The first removal peak in the insulating phase, at -0.2 eV, corresponds to the well screened $3d^1\bar{L}$ state. As explained above, both the $3d^0$ and $3d^1\bar{D}$ states appear roughly at U below the Fermi level. The intra-dimer screening, through the T' hybridization, pushes down the t_{2g} and e_g addition states. But the $d_{||}$ addition state is not affected because it corresponds already to a doubly occupied configuration. The combined result is a shift of the $d_{||}$ addition state to about 1.9 eV towards higher energies. The calculated band gap, approximately 0.9 eV, is in good agreement with the experimental results [4]. The lowest energy charge fluctuations involve transitions from a $3d^1\bar{L}$ to a $3d^2$ state, and the band gap is consequently of the charge-transfer p-d type.

Figure 5 compares the valence band photoemission, taken from Ref. 4, to the calculated spectra (which were broadened by a Gaussian function in order to simulate the experimental resolution). The results of the calculation are in very good agreement with the experimental spectra. The spectra is composed by the V 3d band near the Fermi level, from -2.0 to 0.0 eV and the O 2p band at higher energies, from -8.0 to -4.0 eV. The main changes across the MIT appear in the V 3d band region, whereas the O 2p band does not change much during the transition. The overall spread of the O 2p band transitions is dictated by the value of the $pp\pi$ - $pp\sigma$ parameter.

Figure 6 shows the changes in the V 3d band region across the transition in more detail. In the metallic phase, the spectrum presents the coherent screening peak $3d^1\bar{C}$ around -0.4 eV and the ligand screening part $3d^1\bar{L}$ about -1.6 eV. In the insulating phase, the ligand screening peak appears around -0.9 eV, and the intra-dimer screening part at higher energies. The absence of the coherent feature at the Fermi level in the insulating phase opens the band gap. This shows the relationship between the screening channels and the electronic structure of VO_2 .

Figure 7 compares the O 1s X-ray absorption spectra, taken from Ref. 6, to the calculated spectra. The labels in the spectra indicate the orbitals occupied by the O 1s electron in the final state. The calculated spectra are again in good agreement with the experimental data. In the metallic phase, the structure around 1.0 eV is related to the t_{2g} band and the structure around 3.5 eV to the e_g band (the larger intensity of the e_g band

is due to the stronger hybridization with the O 2p states). The energy separation between the t_{2g} and e_g bands is dictated by the value of the $10Dq$ parameter, whereas the separation of the majority and minority states is determined by the value of the J parameter. The $d_{||}$ band, in the metallic phase, appears around 1.0 eV partially overlapping the t_{2g} band. In the insulating phase, the $d_{||}$ band is shifted approximately to 1.9 eV, towards higher energies. This energy shift of the $d_{||}$ band is mainly determined by the value of the T' parameter. On the other hand, the t_{2g} band does not change and the e_g band presents only a minor shift to higher energies. The evolution of the spectral weight is similar to that observed in the related inverse photoemission spectra [30].

IV. Conclusion

In conclusion, we studied the changes in the electronic structure of VO_2 across the metal-insulator transition. These changes are mainly attributed to differences in the non-local screening processes in each phase. The screening from a coherent state $3d^1\bar{C}$ appears next to the Fermi level (about $\Delta^* \approx 0.6$ eV) in the metallic phase, whereas the screening from the neighbor $3d^1\bar{D}$ appears at higher energies (around $U \approx 4.5$ eV) in the insulating phase. This transfer of spectral weight is responsible for the opening of the band gap in the insulating phase. The structures close to the Fermi level are well screened states, while the true poorly screened state appears at higher energies. These results confirm that the VO_2 compound is in a highly covalent (large T) charge transfer regime ($\Delta < U$).

References

*Corresponding author: miguel@fisica.ufpr.br

1. F. Morin, Phys. Rev. Letters **3**, 34 (1959).
2. M. Imada, A. Fujimori, and Y. Tokura, Rev. Mod. Phys. **70**, 1039 (1998).
3. J.B. Goodenough, J. Solid State Chem. **3**, 490 (1971).
4. S. Shin, S. Suga, M. Taniguchi, M. Fujisawa, H. Kanzaki, A. Fujimori, H. Daimon, Y. Ueda, K. Kosuge, and S. Kachiet, Phys. Rev. B **41**, 4993 (1990).
5. V.M. Bermudez, R.T. Williams, J.P. Long, R.K. Reed, P.H. Klein, Phys. Rev. B **45**, 9266 (1992).
6. M. Abbate, F.M.F. de Groot, J.C. Fuggle, Y.J. Ma, C.T. Chen, F. Sette, A. Fujimori, Y. Ueda, K. Kosuge, Phys. Rev. B **43**, 7263 (1991).
7. M. Abbate, H. Pen, M.T. Czyzyk, F.M.F. de Groot, J.C. Fuggle, Y.J. Ma, C.T. Chen, F. Sette, A. Fujimori, Y. Ueda, and K. Kosuge, J. Electron Spectrosc. **62**, 185 (1993).

8. E. Caruthers, L. Kleinmann, and H.I. Zhang, Phys. Rev. B **7**, 3753 (1973); E. Caruthers and L. Kleinmann, Phys. Rev. B **7**, 3760 (1973).
9. M. Gupta, A.J. Freeman, and D.E. Ellis, Phys. Rev. B **16**, 3338 (1977).
10. R.M. Wentzcovitch, W.W. Schultz, and P.B. Allen, Phys. Rev. Letters **72**, 3389 (1994).
11. T. Uozumi, K. Okada, and A. Kotani, J. Phys. Soc. Jpn. **62**, 2595 (1993).
12. A.E. Bocquet, T. Mizokawa, K. Morikawa, A. Fujimori, S.R. Barman, K. Maiti, D.D. Sarma, Y. Tokura, M. Onoda, Phys. Rev. B **53**, 1161 (1996).
13. A. Fujimori, I. Hase, H. Namatame, Y. Fujishima, Y. Tokura, H. Eisaki, S. Uchida, K. Takegahara F.M.F. de Groot, Phys. Rev. Letters **69**, 1796 (1992).
14. K. Okazaki, H. Wadati, A. Fujimori, M. Onoda, Y. Muraoka, Z. Hiroi, Phys. Rev. B **69**, 165104 (2004).
15. A. Continenza, S. Massidda, and M. Posternak, Phys. Rev. B **60**, 15699 (1999).
16. S. Biermann, A. Poteryaev, A.I. Lichtenstein, and A. Georges, Phys. Rev. Letters **94**, 026404 (2005).
17. A. Liebbesch, H. Ishida, and G. Bihlmayer, Phys. Rev. B **71**, 085109 (2005).
18. R.J.O. Mossaneck and M. Abbate, Solid State Commun. **135**, 189 (2005).
19. T. Saitoh, A.E. Bocquet, T. Mizokawa, H. Namatame, A. Fujimori, M. Abbate, Y. Takeda, M. Takano, Phys. Rev. B **51**, 13942 (1995).
20. G. Zampieri, F. Prado, A. Caneiro, J. Briático, M.T. Causa, M. Tovar, B. Alascio, M. Abbate, E. Morikawa, Phys. Rev. B **58**, 3755 (1995).
21. M. Taguchi, A. Chainani, N. Kamakura, K. Horiba, Y. Takata, M. Yabashi, K. Tamasaku, Y. Nishino, D. Miwa, T. Ishikawa, S. Shin, E. Ikenaga, T. Yokoya, K. Kobayashi, T. Mochiku, K. Hirata, K. Motoya, Phys. Rev. B **71**, 155102 (2005).
22. A. E. Bocquet, T. Mizokawa, A. Fujimori, M. Matoba, and S. Anzai, Phys. Rev. B **52**, 13838 (1995).
23. M.A. van Veenendaal and G.A. Sawatzky, Phys. Rev. Letters **70**, 2459 (1993).
24. K. Okada and A. Kotaki, Phys. Rev. B **52**, 4794 (1995).
25. S.Y. Savrasov, Phys. Rev. B **54**, 16470 (1996).
26. G. Van der Laan, C. Westra, C. Haas, and G.A. Sawatzky, Phys. Rev. B **23**, 4369 (1981).
27. A. Fujimori and F. Minami, Phys. Rev. B **30**, 957 (1984).
28. J.-H. Park, PhD Thesis, The University of Michigan (1993).
29. M.W. Haverkort, Z. Hu, A. Tanaka, W. Reichelt, S.V. Streltsov, M.A. Korotin, V.I. Anisimov, H.H. Hsieh, H.-J. Lin, C.T. Chen, D.I. Khomskii, and L.H. Tjeng, Phys. Rev. Letters **95**, 196404 (2005).
30. A. Tanaka, Physica B **351**, 240 (2004).

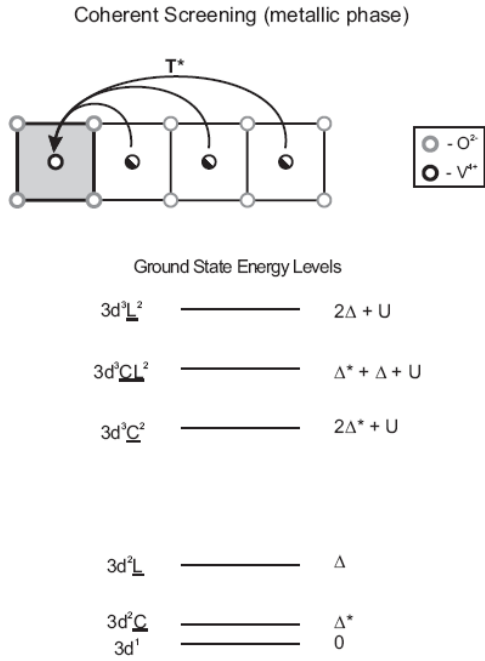


Figure 1: Schematic representation of the coherent screening charge fluctuations (upper) and the energy level diagram of the configurations in the metallic phase (lower).

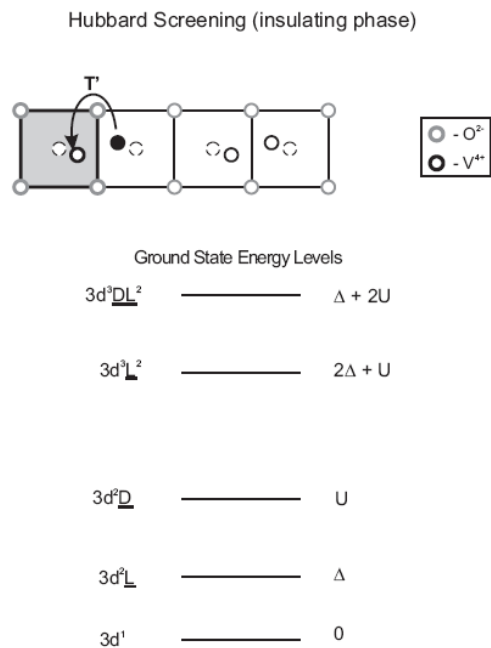


Figure 2: Schematic representation of the Hubbard screening charge fluctuations (upper) and the energy level diagram of the configurations in the insulating phase (lower).

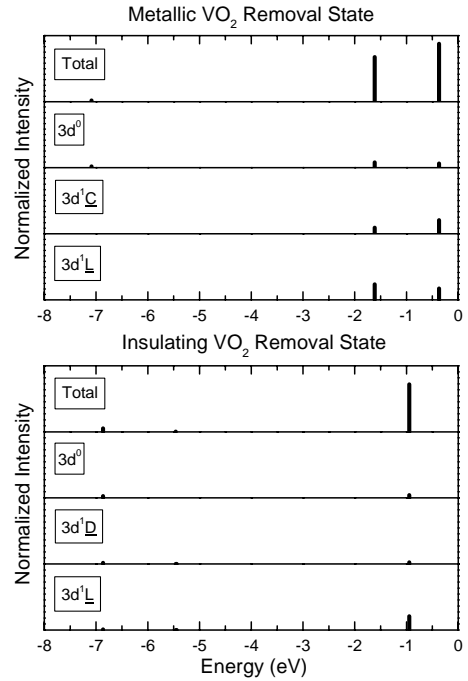


Figure 3: Removal states of metallic and insulating VO_2 decomposed in the main final state configurations.

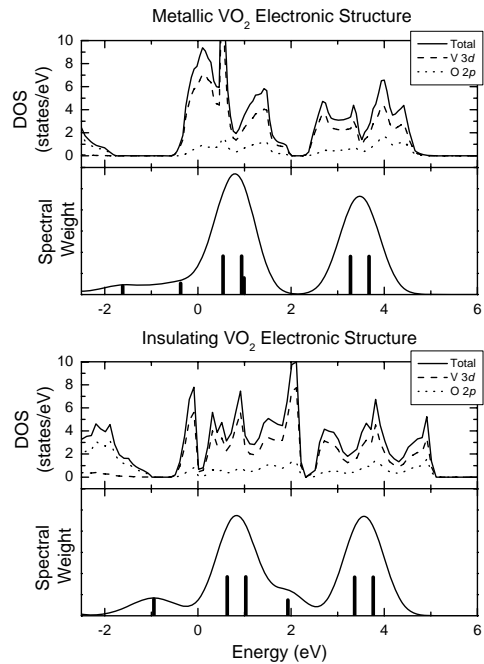


Figure 4: Cluster model calculations of metallic and insulating VO_2 compared to band structure calculations.

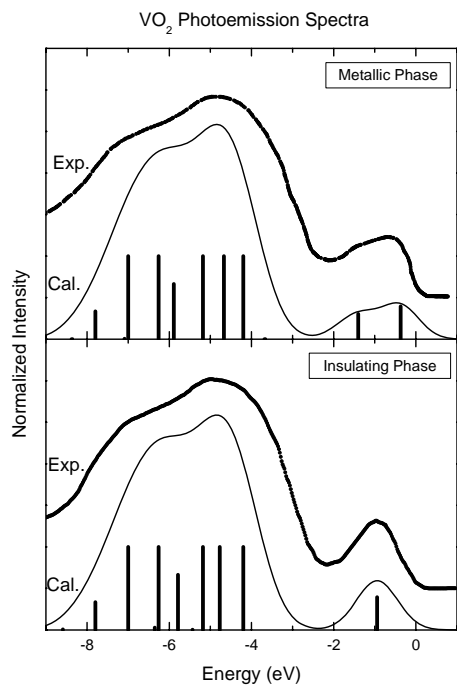


Figure 5: Cluster model calculations of metallic and insulating VO₂ compared to the valence band photoemission spectra taken from Ref. 4.

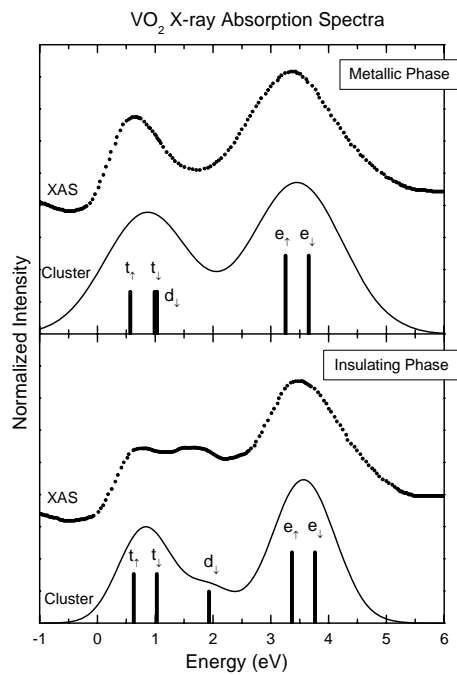


Figure 7: Cluster model calculations of metallic and insulating VO₂ compared to the O 1s X-ray absorption spectra taken from Ref. 6.

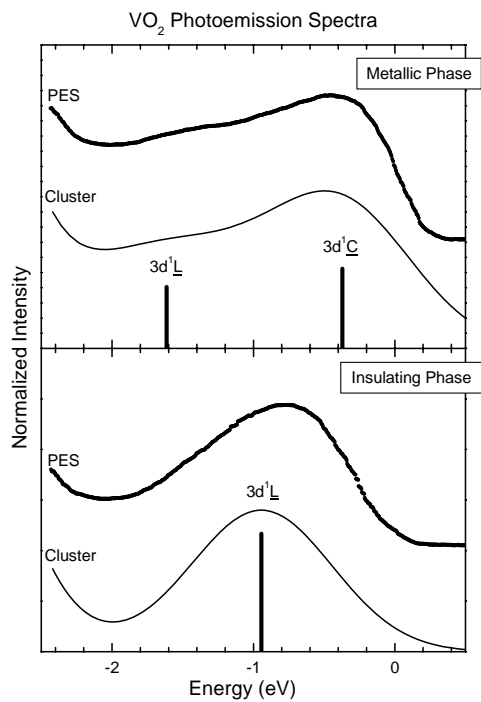


Figure 6: Cluster model calculations of metallic and insulating VO₂ compared to the V 3d region of the photoemission spectra taken from Ref. 4.